Open access • Journal Article • DOI:10.1109/JSTQE.2019.2894067

A Review of Unidirectional Surface Plasmon Polariton Metacouplers

Fei Ding, Sergey I. Bozhevolnyi

Institutions: University of Southern Denmark

Published on: 21 Jan 2019 - IEEE Journal of Selected Topics in Quantum Electronics (Institute of Electrical and Electronics Engineers)

Topics: Surface plasmon polariton and Plasmon

A review of unidirectional surface plasmon polariton metacouplers

Ding, Fei; Bozhevolnyi, Sergey I.

Published in:
I E E E Journal on Selected Topics in Quantum Electronics

DOI:
10.1109/JSTQE.2019.2894067

Publication date:
2019

Document version:
Accepted manuscript

A Review of Unidirectional Surface Plasmon Polariton Metacouplers

Fei Ding, and Sergey I. Bozhevolnyi

***Abstract*—Efficient and unidirectional excitation of surface plasmon polaritons (SPPs) and their low-frequency counterparts (i.e., spoof SPPs) is highly desired in the research area of photonics and plasmonics, while being at the same time rather challenging. Recent progress in gradient metasurfaces, ultrathin and planar materials composed of sub-wavelength unit cells, has opened up new possibilities for efficiently coupling of free-space propagating waves to surface waves. In this paper, we will discuss the recent achievements in gradient metasurface-based unidirectional SPP couplers (i.e., metacouplers). Starting with explaining the basic concept of generalized Snell's law, we then introduce some typical examples of unidirectional SPP metacouplers, followed by an overview of polarization-controlled tunable SPP metacouplers. We also describe metacouplers that also feature other functionalities, beyond the unidirectional SPP excitation. The review is concluded with a short summary and perspective for future developments.**

***Index Terms*—Metacoupler, generalized Snell's low, PB-phase, polarization-controlled, multifunctional**

I. Introduction

SURFACE plasmon polaritons (SPPs), propagating along metal-dielectric interfaces excitations that arise from the coupling of light with collective oscillations of free electrons, have attracted a great deal of attention in the research areas of physics, chemistry, biology, and material science due to their unique properties, notably, ultimate (below the diffraction limit) field confinement along with its significant enhancement [1]–[4]. In low-frequency regions where natural SPPs don't exist, spoof SPPs on nanostructured metals can also find numerous exciting applications [5]–[8]. Despite all the progress and developments in SPP applications, efficient and unidirectional SPP excitation remains one of the most challenging issues because of the inherent momentum mismatch between the propagating waves (PWs) and surface waves (SWs), which forbids the direct coupling between them. Typically, prisms and gratings are used to excite SPPs in a predesigned direction. However, the conventional approaches are rather limited in controlling the directions of generated SPPs since the efficient SPP excitation requires accurate phase matching and incident beam positioning, strict requirements that inevitably limit practical applications [1], [9]. Worse still, prisms are too bulky and not suitable for coupling light to compact plasmonic devices. In this regard, compact SPP couplers that can efficiently and unidirectionally excite SPPs from normally incident PWs are highly desirable in photonic and plasmonic integration.

Recently, gradient metasurfaces, i.e., planar artificial surfaces made up of properly arranged resonant subwavelength elements that enable arbitrary control over the electromagnetic (EM) waves, have attracted the progressively increasing attention, becoming a rapidly growing field of research that provides promising solutions for low-cost, ultra-compact and high-performance EM devices [10]–[22]. Distinct from conventional EM devices that modulate the EM wave via gradually accumulated phase changes during wave propagation, gradient metasurfaces can engineer the amplitude, phase, and polarization locally by directly modifying the boundary conditions. As such, gradient metasurfaces can mimic bulk EM devices, and numerous flat functional components have been accordingly demonstrated, such as beam steerers [10], [23]–[27], metalenses [28]–[36], holograms [37]–[43], waveplates [44]–[48], and polarimeters [49]–[55].

In addition to manipulating PWs in free space, gradient metasurfaces also show unprecedented capabilities of unidirectionally coupling SWs from PWs. In this paper, we review the recent achievements in a specific branch of gradient metasurface-based applications — unidirectional SPP metacouplers. The rest of this paper is organized in the following sections. In Section II, we first explain the basic concept of generalized Snell's law and then introduce the configurations suitable for realization of unidirectional SPP metacouplers. Section III is concentrated on polarization-controlled tunable SPP metacouplers. In Section IV, we describe metacouplers that can operate for other (than the unidirectional SPP excitation) functionalities. Finally, we summarize and provide perspective for future developments in Section V. In passing, we would like to mention that this review mainly focuses on the unidirectional SPP metacouplers based on gradient metasurfaces. Thus we don't discuss some nice demonstrations of unidirectional SPP couplers that rely on slits and/or integrated asymmetric grooves [56]–[58], aperiodic grooves or antennas with optimized dimensions [59]–[62]. Additionally, we don't involve some nice demonstrations of unidirectional SPP emission using a single emitter, which is also very promising for integrated photonics [63]–[65].

This work was supported in part by the European Research Council, Grant 341054 (PLAQNAP) and the University of Southern Denmark (SDU 2020).

Fei Ding and Sergey I. Bozhevolnyi are with SDU Nano Optics, University of Southern Denmark (e-mail: feid@mci.sdu.dk).

II. Principle and Unidirectional SPP Metacouplers

A. Phase Discontinuities and Generalized Snell's Law

When a plane EM wave encounters a planar interface between different homogeneous media, reflection and refraction will take place simultaneously, and the directions of reflected/transmitted beams are determined by Snell's law based on the boundary condition of the EM theory. However, if phase discontinuity is introduced at the interface by properly-arranged subwavelength resonant antennas that form a gradient metasurface, the reflections and refractions will be different since the boundary condition is modified, thereby creating the so-called generalized Snell's law [10], [24]. Fig. 1 schematically illustrates the three-dimensional (3D) system used to derive the generalized Snell's law of reflection and refraction, where a phase gradient $\frac{d\Phi}{dr}$ is introduced along the interface. Base on Fermat's principle, the generalized Snell's law in this 3D case can be written as [10], [24]:

$$\begin{cases} n_t \sin(\theta_t) - n_i \sin(\theta_i) = \frac{\lambda_0}{2\pi}\frac{d\Phi}{dx} \\ n_t \cos(\theta_t)\sin(\varphi_t) = \frac{\lambda_0}{2\pi}\frac{d\Phi}{dy} \end{cases}. \quad (1)$$

$$\begin{cases} n_i \sin(\theta_r) - n_i \sin(\theta_i) = \frac{\lambda_0}{2\pi}\frac{d\Phi}{dx} \\ n_i \cos(\theta_r)\sin(\varphi_r) = \frac{\lambda_0}{2\pi}\frac{d\Phi}{dy} \end{cases}. \quad (2)$$

where n_i and n_t are the refractive indexes of two media, $\frac{d\Phi}{dx}$ and $\frac{d\Phi}{dy}$ are the x- and y-component of the phase gradients, λ_0 is the wavelength in free space, and θ_i, θ_r and θ_t are the incident, reflected, and refracted angles respectively. From equations (1)-(2), one may notice that the reflected and refracted beams can have arbitrary directions in the 3D space given a suitable phase gradient is provided. When the phase gradient perpendicular to the incident plane equals to zero, namely, $\frac{d\Phi}{dy} = 0$, this 3D situation becomes two-dimensional (2D). Therefore, equations (1)-(2) can be written as

$$n_t \sin(\theta_t) - n_i \sin(\theta_i) = \frac{\lambda_0}{2\pi}\frac{d\Phi}{dx}. \quad (3)$$

$$n_i \sin(\theta_r) - n_i \sin(\theta_i) = \frac{\lambda_0}{2\pi}\frac{d\Phi}{dx}. \quad (4)$$

As a consequence, the relation between θ_i and θ_r becomes nonlinear, distinct from the conventional case that θ_i and θ_r are identical. Importantly, there is always a critical incident angle of $\theta_c = \sin^{-1}\left(1 - \frac{1}{n_i}\frac{\lambda_0}{2\pi}\left|\frac{d\Phi}{dx}\right|\right)$, above which the reflected light becomes evanescent. In this regard, when the phase gradient $\frac{d\Phi}{dx}$ of a certain metasurface is large than free-space wavevector, the wave "reflected" by the metasurface is a SW instead of a PW, which forms the basic theory of gradient metasurface-based SPP coupler. Additionally, since the phase gradient provide by metasurfaces is usually unidirectional, asymmetric SPP excitation can be easily achieved at normal incidence.

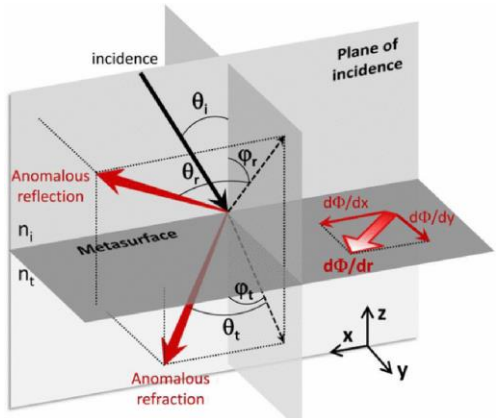

Fig. 1. Schematic of a 3D system with an interfacial phase gradient $\frac{d\Phi}{dr}$ providing an effective wavevector along the interface that can bend the transmitted and reflected light into arbitrary directions. [13].

B. Unidirectional SPP Metacouplers

As discussed previously, the anomalous reflection disappears and directional SWs will be driven along the gradient metasurface when the parallel phase gradient is larger than the wavevector in free space. In 2012, Zhou and co-workers first proposed a metacoupler that enables coupling a free-space PW into a SW with nearly 100% efficiency [66]. In the design, metal-insulator-metal (MIM) meta-atoms were used to realize 2π phase span for reflected field, thereby forming various metasurfaces with different phase gradients [Fig. 2(a)]. When the phase gradient is larger than the free-space wavevector, symmetric coupling between PWs and SWs occurs, and consequently the far-field reflection vanishes, as shown in Fig. 2(b). Since the metasurface is spatially inhomogeneous, no eigen guided mode is support. Therefore the generated SW on the metasurface is not an eigen SPP mode. In order to guide the SWs out, the authors placed a properly-designed mushroom metasurface which supports the eigen-SPP-like mode at the side of the gradient metacoupler. Based on the near-field scanning technique, the near-field pattern of the generated SWs was mapped out, indicating the unidirectional SPP excitation [see Fig. 2(c) and 2(d)]. Importantly, this nearly perfect PW-SW conversion can be achieved at any angle larger than the critical angle as the momentum mismatch between PWs and SWs is compensated by the reflection phase gradient, which is different from the prisms or gratings couplers relying on resonant critical coupling [1]. However, it should be mentioned that the claimed perfect PW-SW conversion is limited to ideal gradient

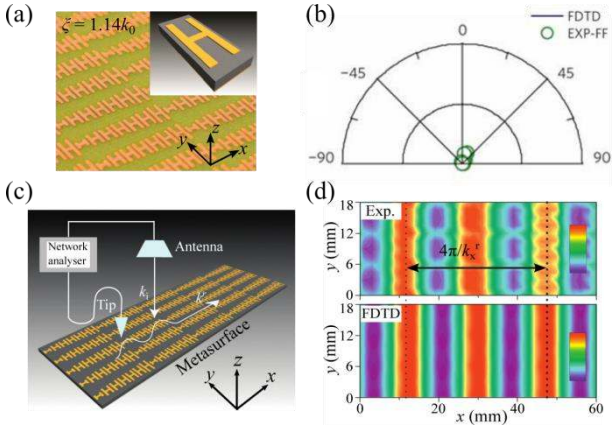

Fig. 2. Unidirectional SPP metacoupler in the microwave range. (a) Schematic of the gradient metasurface composed of MIM meta-atoms. (b) Simulated and measured far-field scattering patterns of the metacoupler. (c) Schematic of the PW-SW coupling on a gradient metasurface probed by near-field scanning technique. (d) Near-field measured (top) and simulated (bottom) E_z distributions on part of the metasurface with phase gradient $\xi = 1.14k_0$ under the excitation of an x-polarized wave at normal incidence. [66].

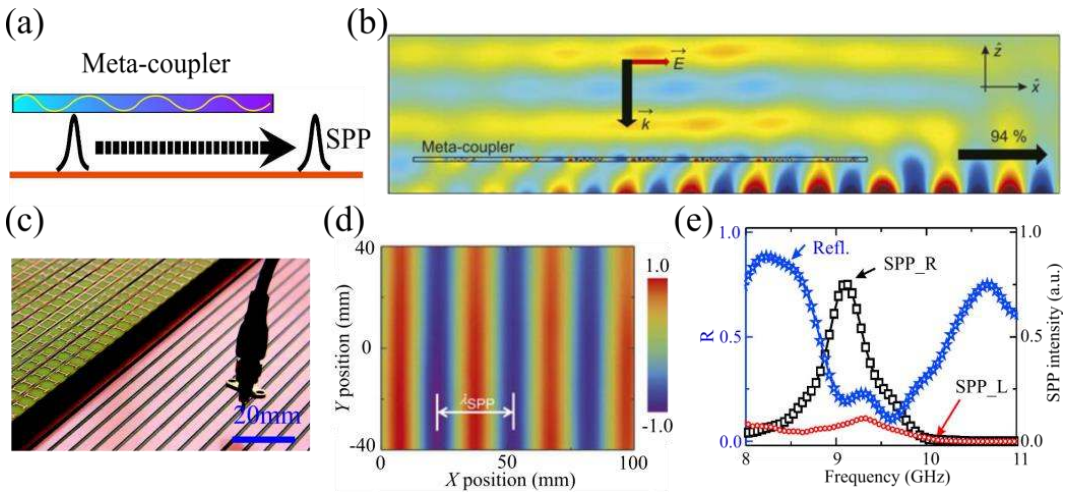

Fig. 3. Novel highly-efficient unidirectional SPP metacoupler. (a) Schematic of the new configuration for highly-efficient SPP excitation which consists of a transparent gradient metasurface placed at a certain distance above the target plasmonic metal. (b) Simulated H_y field distribution in the case of SPP excitation by designed metacoupler in an optimized configuration, showing that the highest SPP coupling efficiency is 94%. (c) Image of part of fabricated sample and the experimental setup for near-field mapping. (d) Near-field measured real part of E_z field distribution on the plasmonic metal composed of mushroom structures. Here the meta-coupler is illuminated by an x-polarized wave at the frequency of 9.2 GHz and the incident angle is around 8°. (e) Measured spectra of the integrated reflection and intensities of the generated spoof SPPs propagating in different directions. [70].

metasurface and the side-coupling configuration only works well for excitation light with small beam size [67]. The conversion efficiency decreases significantly when the size of incident beam is increased, which is ascribed to the significant scattering caused by inter-supercell discontinuities. In this regard, the gradient metasurface constructing the metacoupler should be purposely designed and optimized.

Here it should be noted that this metacoupler approach can be extended to unidirectionally couple waveguide modes from free-space incident light [68], [69].

C. *Novel Highly-efficient Unidirectional SPP Metacoupler*

In order to solve the issue of degraded coupling efficiency due to decoupling of SPPs back to PWs by the non-negligible scattering within the inhomogeneous metacoupler and at the side-boundary between the metacoupler and the plasmonic interface supporting eigen SPP mode, a new configuration of unidirectional SPP excitation has been proposed and experimentally demonstrated by Sun et al. recently, which is composed of a transparent gradient metasurface placed on top a plasmonic interface with an optimized distance [70]. Fig. 3(a) illustrates the working principle: when the incident light impinges on the top surface of the metacoupler, the incident light is first converted into a driven SW on the gradient metasurface without any reflection, and then the SW tunnels down and transfers its energy to the eigen SW mode of the bottom plasmonic metal (i.e., spoof SPPs in microwave range). As such, the surface reflections and the decoupling of SWs back to PWs are greatly suppressed, thereby resulting in high-efficiency SPP conversion. As shown in Fig. 3(b), when the distance between the topmost transparent metasurface and the bottom plasmonic metal is optimized at a particular value where the two competing process of excitation and scattering are balanced, the numerically calculated SPP coupling efficiency reaches as high as 94%. To validate the design, a proof-of-concept metacoupler in the microwave regime was designed and fabricated, which consists of multilayered sandwich structures with the transmission amplitude of nearly 100% and the transmission phase covering the entire 2π range. In the microwave experiment, the fabricated metacoupler was placed at an optimized distance of d_c = 10 mm above the plasmonic metal composed of mushroom structure that supports the spoof SPPs [Fig. 3(c)]. After both the near-field and far-field characterizations, the spoof SPP coupling efficiency was found to be around 73%, which is much higher than those of all other available devices operating in this frequency domain [see Fig. 3(d) and 3(e)].

III. Polarization-controlled Tunable SPP Metacouplers

The SPP metacouplers that have been discussed above are all about coupling PWs to SWs in a predefined direction. In this regard, the direction of generated SPPs is fixed and cannot be switched, which is not compatible with the requirements of tunability and reconfigurability in modern plasmonic circuits and systems. Therefore, the subject of polarization-controlled SPP excitation has become a new frontier of metasurface research recently. In this section, we will review some of the research progress in polarization-controlled SPP metacouplers.

A. *Spin-controlled Tunable SPP Metacouplers*

To start with, we first show some examples of spin-controlled SPP metacouplers based on properly-arranged nanoapertures in an opaque metal film, in which the SPP excitation direction can be controlled by the spin of the incident circular-polarized (CP) light [71]–[74].

Fig. 4(a) displays the proposed spin-controlled tunable directional SPP coupler by Capasso and co-workers, which is composed of periodic elongated rectangular apertures in metal film [71]. When the light is incident on a subwavelength aperture with the electric field polarized perpendicular to the narrow aperture, SPPs are generated and transmitted through the apertures to the other side of the metal film and the SPP emission pattern is approximately that of an in-plane dipole [75]. Thus, by arranging such apertures in a column with a subwavelength distance smaller than the SPP wavelength, SPP

plane waves are formed and then propagating perpendicularly away toward either side of the column, which is independent of the orientation of the apertures within the column. Based on such SPP plane waves, complicated polarization response can be realized through the interferences of the SPP waves generated by multiple columns with certain orientations. Therefore, spin-dependent SPP excitation can be achieved by positioning two columns in a spacing that equals to a quarter of the SPP wavelength and orienting the corresponding apertures in each column at 90° with respect to each other [Fig. 4(a)]. Consequently, the interference of SPP plane waves becomes dependent on the incident spin instead of the linear-polarization, resulting in spin-controlled tunable directional SPP coupling. In the experiment, 10 column pairs were fabricated using focused ion beam (FIB) milling to increase the coupling efficiency of SPP excitation though one column pair can work properly in principle [Fig. 4(b)]. Fig. 4(c) shows the near-field scanning optical microscopy (NSOM) images of the device under illumination with different polarization states at λ = 633 nm, indicating the spin-selective excitation of SPP waves. For example, the right CP (RCP) light mainly generates right-propagating SPP beam while the SPPs to the left side are greatly suppressed. Once the incident light is switched to left CP (LCP), most of the SPP waves are routed to the left side. On the contrary, the linearly-polarized light will create SPPs with equal intensities towards either side of the metacoupler. Following this concept, polarization-selective coupling from an optical fiber to long-range SPP waveguide modes was demonstrated by using plasmonic antenna arrays embedded in polymer cladding, which allows for the sorting of two distinct polarizations to counter-propagating SPP waveguide modes [76].

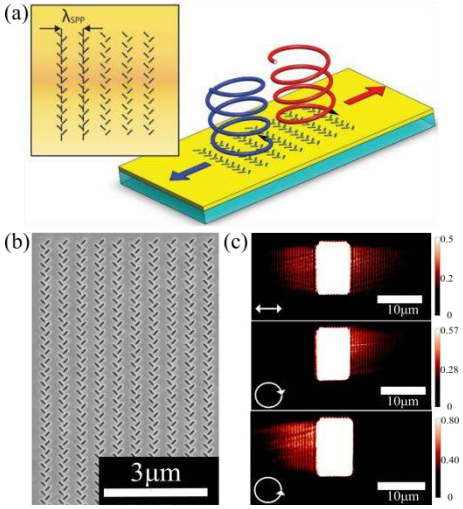

Fig. 4. Spin-controlled tunable directional SPP coupler based on interference. (a) schematic of the column pairs of subwavelength apertures as spin-controlled SPP coupler. (b) Scanning electron microscope (SEM) images of the fabricated sample in a gold film. (c) NSOM images of the device under illumination with different polarization states at λ = 633 nm. [71].

In the previous examples, the spin-controlled tunable SPP excitation is achieved by the interference between neighboring subwavelength apertures [71] or within the designed aperture [74]. An alternative approach to realizing spin-controlled SPP excitation is to use the so-called Pancharatnam-Berry (PB) or geometric phase metasurface, which provides a spin-sensitive phase gradient with opposite sign when the metasurface is illuminated with different CP light [77]–[81]. Based on PB-phase, spin-controlled tunable SPP metacouplers have been proposed based on arrays of apertures [82]–[85]. In 2013, Zhang and co-workers demonstrated a compact spin-dependent directional SPP metacoupler to selectively excite SPPs along opposite directions at normal incidence in the near-infrared range [see Fig. 5(a)] [82]. In the design, both the spin-sensitive phase gradient $2\sigma\Delta\phi/s$ provided by the rotated apertures and the reciprocal vector of lattice $2m\pi/s$ are utilized to compensate the SPP wavevector k_{SPP}, where σ is the incident spin, $\Delta\phi$ is the step of rotation angle between neighboring apertures, s is the period of the apertures, and m is a integer representing the order. Thus, unidirectional SPPs can only be generated when the conditional of phase (or momentum) matching is fulfilled: $k_{SPP} = 2\sigma\Delta\phi/s + 2m\pi/s$, thereby resulting in asymmetric matching when different spin σ is involved. From Fig. 5(b), one can see that the phase matching condition is shifted to a higher frequency of ω_1 and the SPPs will propagate along the $+x$-direction when $\sigma = +1$. Once the spin σ is switched to -1, the phase matching condition is still met at ω_1 while the direction of excited SPPs will become opposite to the $-x$-direction. Similarly, spin-controlled tunable SPP excitation can be achieved at a lower frequency of ω_3. As shown in Fig. 5(c), the propagating direction of the generated SPPs can be switched to the opposite sides when the incident spin is altered at the design wavelengths of λ = 780 and 1020 nm. However, the SPPs have equal intensity at λ = 870 nm regardless of the incident spin, which is ascribed to the fact that the phase matching is realized by the reciprocal vector of lattice in the first-order instead of the PB-phase possessing spin-dependent sign. Once this one-dimensional (1D) lattice is extended to complicated 2D lattices, such as inverse asymmetric 2D Kagome lattice, spin-controlled SPP launching can be realized in multiple directions [85].

In the above aperture-based configuration, the coupling efficiency of SPP excitation is relatively low as most of the incident light transmits directly through the apertures and thus be wasted. To increase the efficiency, gap-surface plasmon (GSP) PB-phase metasurfaces have been proposed to demonstrate spin-controlled SPP excitation [20], [86]. For example, a polarization-tunable SPP coupler based on GSP PB-phase metasurface has been demonstrated, where the phase matching was fulfilled by combining the spin-controlled PB-phase and reciprocal vector of lattice [86]. Specifically, the metacoupler is composed of arrays of gold brick-shaped nanoantennas with a local phase discontinuity on top of a continuous gold film separated by a dielectric space [Fig. 5(d)]. Fig. 5(e) displays the recorded images scattered by two out-coupling grating milled on the sample surface for three different incident polarization states, manifesting the polarization-selective SPP excitation. Once the polarization state of incident light is continuously tuned by rotating the quarter-wave plate, the integrated intensity from two gratings varies correspondingly, as shown in Fig. 5(f). For the circular polarizations, unidirectional SPP excitation is observed while

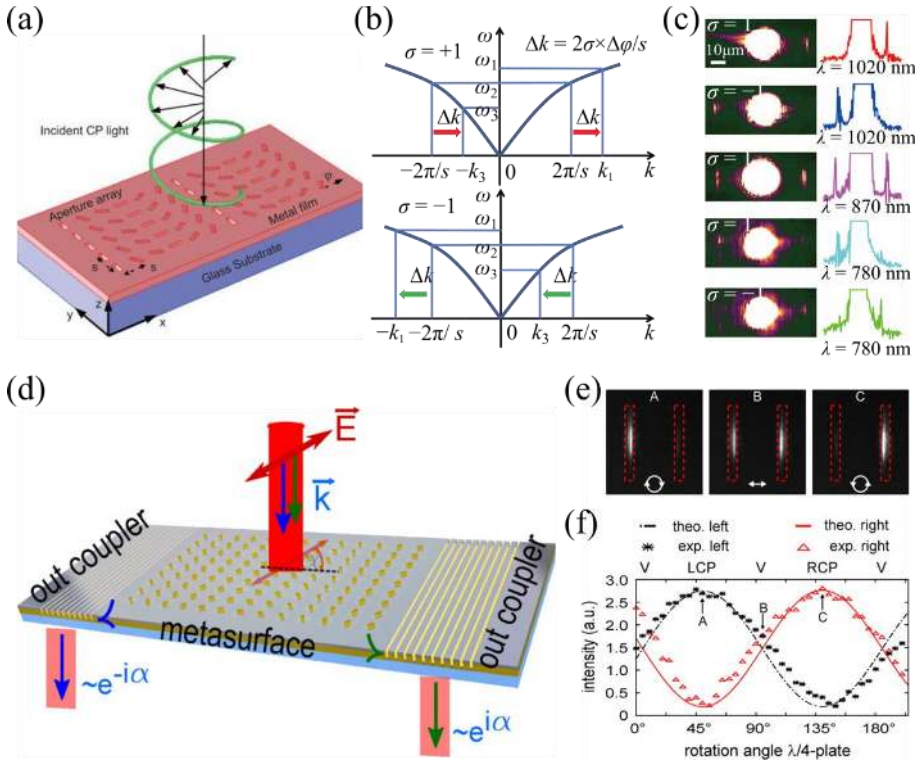

Fig. 5. Spin-controlled tunable directional SPP metacouplers based on PB-phase. (a) schematic of the unidirectional SPP coupler composed of rectangular apertures with local orientations on a metal film. (b) Dispersion curve of SPPs and the phase matching condition for ordinary and anomalous diffraction orders. (c) Experiment demonstration of wavelength-selective unidirectional SPP excitation. [82]. (d) Schematic of the GSP PB-phase metasurface for selective SPP excitation. (e) Recorded images scattered by two out-coupling grating for three different incident polarization states. (f) Integrated intensity from the right (red triangles) and left (black stars) gratings over the rotation angle of the quarter-wave plate. [86].

the other polarization states allow for arbitrary tuning the amplitudes of the two counter-propagating SPPs. Here the calculated excitation efficiency of SPPs reaches nearly 4% at λ = 800 nm, which is still far from satisfactory.

Although the aforementioned PB-phase metasurfaces can realize direction-controlled SPP excitation, such approach suffers from low-efficiency due to several issues. First, the specular reflection from the PB-phase coupler is always there and cannot be eliminated, thus wasting a large portion of the incident energy. Second, there are polarization mismatch between the excitation source and the SPP modes supported in the infinite dielectric-metal interface since the incident CP light has both TE and TM components while the SPP mode is TM-polarized, thereby inducing significant scattering and subsequently decreasing the coupling efficiency. Additionally, the SPP mode generated in the metacoupler is slightly different from the eigenmode supported in the plasmonic structure, which causes non-negligible scattering at the boundary. Very recently, a new method of SPP coupling has been proposed and demonstrated to achieve highly-efficient spin-controlled SPP excitation in the microwave, which have solved all the aforementioned issues, shown in Fig. 6(a) [87]. In this approach, the PB-phase metasurface is carefully designed to couple incident CP wave into a driven SW with the efficiency reaching as high as 100%, which only uses PB-phase to match the wavevector of SWs, different from previous studies. In particular, the meta-atoms constructing the metasurface behave as high-efficiency half-wave plates operating in reflection geometry, thus ensuring near 100% efficiency to convert a CP PW to a SW. Moreover, the air-metal interface is properly designed to support both TM and TE-polarization-like spoof SPPs. From the simulation results shown in Fig. 6(b), one can clearly observe the spin-controlled SPP excitation, where the metacoupler is illuminated by a CP Gaussian beam at normal incidence. The E_x and E_y field distributions validate the excitation and propagation of TE- and TM-polarized spoof SPPs, respectively. Regarding the microwave experiments, near-field characterization was first conducted by near-field

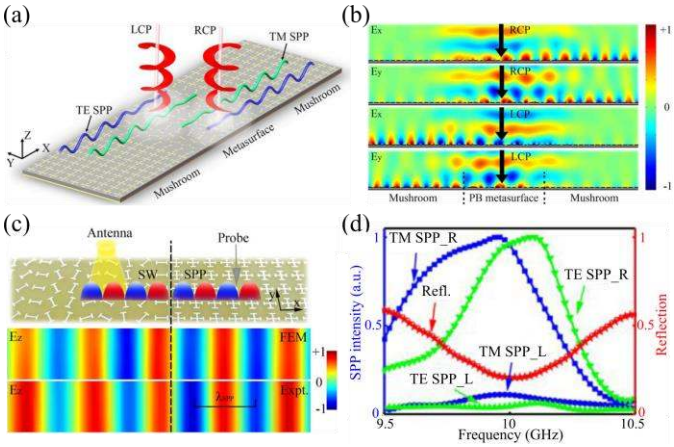

Fig. 6. Highly-efficient spin-controlled SPP coupler with PB metasurface (a) Schematics of the designed metacoupler illuminated by the LCP or RCP waves, producing high-efficiency spin-controlled SPPs. (b) Simulated real part of E_x and E_y field distributions inside the SW metacoupler illuminated by a normally incident RCP or RCP wave. (c) Near-field characterizations of the high-efficiency PB metacoupler. (d) The integrated total reflection and the excited SPP intensities above the left-side and right-side mushrooms [87].

scanning technique, in which two small antennas were adopted to probe the E_z and H_z components of the local fields, manifesting clearly the generation of both TE- and TM-polarized driven SWs on the PB-phase metasurface [Fig. 6(c)]. Compared to the simulated results, the experimental results show perfect agreement. After integration and calculation, the SPP excitation efficiency is found as high as 78% and can be even further improved to 92% with an optimized condition [Fig. 6(d)]. Importantly, the direction of excited SWs can be switched by changing the helicity of the incident CP wave.

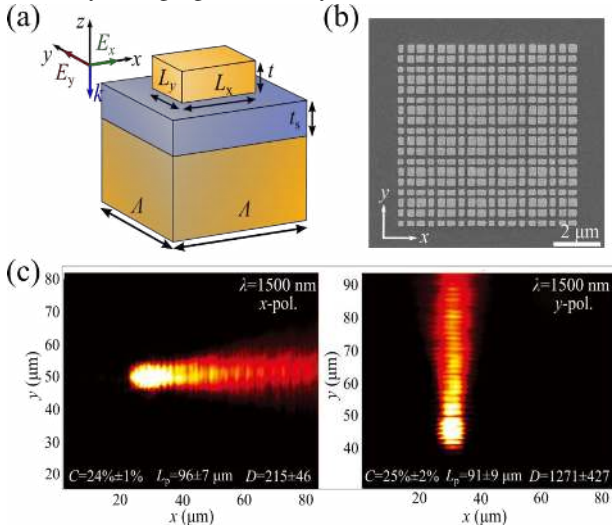

Fig. 7. Linear-polarization-controlled tunable SPP metacoupler. (a) Sketch of a basic GSP unit cell. Middle panel: (b) SEM image of fabricated 2D-periodic polarization-sensitive SPP coupler composed of 6 × 6 supercells. (c) Recorded LRM images for two different polarizations at λ = 1500 nm. In each image, the coupling efficiency C, propagation length L_P, and directivity D are indicated. [88].

B. Linear-polarization-controlled Tunable SPP Metacoupler

In addition to spin-controlled tunable SPP excitation, linear-polarization has also been used to demonstrate switchable and unidirectional SPP generation, which shows the advantage of ease of integration as no quarter-wave plate is involved [88]. Here we would like to highlight a GSP-based metacoupler that is capable of efficiently converting incident light with arbitrary polarization into SPPs propagating in orthogonal directions. The metacoupler consists of GSP resonators arranged in a periodic manner, thereby producing two independent orthogonal linear phase gradients for reflected fields in both x- and y-polarizations, which can compensate the momentum mismatch between the PWs in free space and bounded SPPs. As shown in Fig. 7(a), the basic GSP meta-atom is composed of topmost gold nanoantennas and an 80-nm-thick continuous gold film, separated by a 50-nm-thick SiO_2 insulating layer. In the experiment, 6 × 6 supercells were fabricated to form the 2D-periodic linear-polarization-sensitive SPP coupler operating at telecom wavelength [Fig. 7(b)]. Fig. 7(c) displays the recorded images from leakage radiation microscopy (LRM) at the design wavelength of λ = 1500 nm, indicating the linear-polarization-controlled excitation of SPPs with a high directivity. By integrating the LRM images, the coupling efficiency for both polarization was found to be ~ 25%, which is a little lower than the predicted value of 40%. For both polarizations, almost all the SPPs power goes in the designed direction and the measured directivities are more than 150. Since the phase response of GSP metasurface is broadband, such polarization-controlled metacoupler can work over a wide spectrum ranging from 1500 nm to 1600 nm with reasonable performance. Very recently, this type of linear-polarization-controlled SPP coupler has been combined with spin-controlled coupler to realize an in-plane polarimeter, where the incident light is converted into SPP waveguide modes propagating to six different directions [89]. By integrating the coupling efficiency of SPP wave modes in the predefined six directions, the polarization state of incident light can be determined.

IV. Multifunctional Metacouplers Beyond Unidirectional SPP Excitation

In the previous sections, the unidirectional SPP metacouplers are designed only for the single functionality of SPP launching in desired directions, not quite reaching the goal of integration and miniaturization in plasmonics and microwave systems, which requires integrating multiple diversified functionalities into a single compact device. Therefore multifunctional metacouplers beyond unidirectional SPP excitation have become an emerging research area. In this section, we will review some of the recent progress in multifunctional metacouplers possessing distinct functionalities, one of which is related to unidirectionally generate SPPs in the near field.

A. Linear-Polarization-Controlled Bifunctional Metacouplers

As a good example, Fig. 8(a) and 8(b) schematically shows the first demonstration of a reflective multifunctional metacoupler possessing two distinct functionalities of simultaneous focusing and PW-to-SW conversion in the microwave regime. Similar to the linear-polarization-controlled SPP excitation [88], this reflective bifunctional microwave metasurface uses strongly anisotropic MIM structure as the basic meta-atom, which provides arbitrary phase and amplitude control over the reflected light under the excitation of linearly-polarized wave [90]. By carefully adjusting the geometrical parameters of each meta-atom, the certain metasurface to achieve special wavefront control can be accordingly designed, which exhibits desired linear-polarization-dependent phase profiles [i.e., $\varphi_{xx}(x,y)$ and $\varphi_{yy}(x,y)$] on the 2D x-y grid. Fig. 8(a) and 8(b) displays the hyperbolic phase and the linear phase profile for the y-polarized and x-polarized incident wave, respectively. When a y-polarized microwave at the design frequency of f = 9.3 GHz is normally incident on the sample, the incoming plane wave will be reflected and focused to a focal point at f = 94 mm, which matches well with the theoretical design (f = 90 mm), as shown in Fig. 8(c). At the focal point, the EM field is strongly enhanced. Additionally, the good performance of focusing is sustained in the frequency range of 8.4 – 11.2 GHz, where the focal-spot size varies in the range of 31 – 37 mm and the focal length changes between 86 and 115 mm. Since the loss in microwave range is rather low, the working efficiency of this meta-lens, which is defined by the ratio between the powers confined in the focal spot and carried by the incident beam, surpass ~ 90.8% at the designed working frequency of f = 9.3 GHz. Once the incident light is switched to x-polarized, the

phase gradient ξ_x along the x-direction supplied by the gradient metasurface is larger than free-space wavevector k_0 and can be perfectly matched with the wavevector of the eigen spoof SPPs supported by the designed mushroom structure [66]. Thus the driven SWs on the metacoupler can be effectively guided out and propagate over the mushroom structure. The measured near-field pattern represents a very well-defined spoof SPP with k_{SPP} = 206.5 m^{-1}, which is in good agreement with the theoretically calculated value of k_{SPP} = 209.4 m^{-1} [see Fig. 8(c)]. More importantly, the absolute PW-SW conversion efficiency is measured to be about 90%, which is in good agreement with the simulation value of 92%.

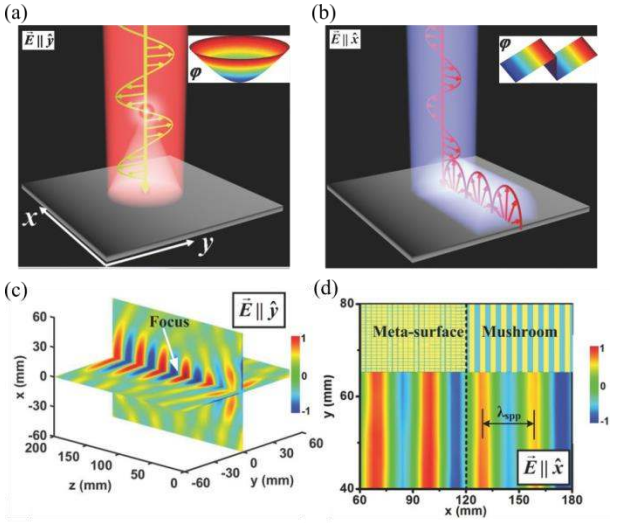

Fig. 8. Reflective bifunctional metacouplers in the microwave range. (a,b) Schematics and working principles of the reflective bifunctional metasurface which behaves as a focusing lens (a) and a PW-SW convertor (b) when excited by y- and x-polarized light, respectively. (c) Measured real part of electric distributions on both xoz and yoz planes as the metacoupler is illuminated by a normally incident y-polarized plane wave at f_0 = 9.3 GHz. (d) Measured real part of electric pattern E_z on the xy-plane using a monopole antenna placed vertically and 8 mm above the metasurface and the mushroom structure, under the illumination of a normally incident x-polarized plane wave at f_0 = 9.3 GHz. [90].

While metacouplers possessing dual-functionalities of unidirectional PW-SW conversion and free-space wavefront shaping have been successfully demonstrated in the microwave region, it is highly-desired to realize similar metacouplers working in the optical range, which may have the great potential applications in realistic plasmonic and photonic integration. Very recently, a visible bifunctional GSP metasurface that enables simultaneous polarization-controlled unidirectional SPP excitation and beam steering at normal incidence has been proposed and demonstrated [91]. As shown in Fig. 9, the proposed visible bifunctional metacoupler possesses two different linear phase-gradients (i.e., ζ_x and ζ_y) along the same direction (i.e., x-direction) in respective two linear polarizations, thereby allowing for efficiently converting x-polarized radiation into SPPs supported in the plasmonic interface and anomalously steering the reflected light for y-polarization simultaneously. In this regard, the reflection phase-gradient for x-polarization is equal to the wavevector of excited SPPs bounded on the air-dielectric-metal interface (i.e., $\zeta_x = k_{SPP}$), while the phase-gradient is smaller than the wavevector of propagating light in free space when the incident light is y-polarized (i.e., $\zeta_y < k_0$). Specifically, the supercell is composed of six anisotropic GSP elements [gray area in Fig. 9(a)], which provides a 4π phase span with a constant phase shift of 2π/3 between the neighboring elements for x-polarization. However, the supercell provides only a 2π phase span for y-polarization. As such, the proposed visible bifunctional GSP metacoupler functions as phase grating with different periodicities respect to the incident linear polarizations along the x-direction. Fig. 9(b) displays the SEM image of the fabricated three-component device for SPP excitation, which consists of the SPP metacoupler in the center and two identical decoupling gratings on the right- and left-side for out-coupling the SPPs into free space photons. In the experiment, a tightly-focused x-polarized Gaussian beam with the beam waist of w = ~ 2 μm was incident on the SPP metacoupler. After optimizing the position of the incident beam, the coupling efficiency of the right-propagating SPPs was maximized, resulting in high-efficiency unidirectional SPP excitation. It's remarkable that unidirectional excitation of SPPs was observed in a broadband wavelength range from 600 to 650nm, in which the averaged coupling efficiency C_r is larger than 25%, shown in Fig. 9(b). Additionally, the measured extinction ratio ER surpasses 20 dB in the investigated spectral range of 600 – 650 nm. Besides the unidirectional SPP excitation for normally incident light polarized in the direction of the phase gradient, the designed metacoupler functions as an efficient beam-steerer when the normally incident light is polarized perpendicularly to the phase gradient direction. From Fig. 9(c), one can clearly see that most of the light is anomalously routed to the +1 diffraction over a wide spectrum

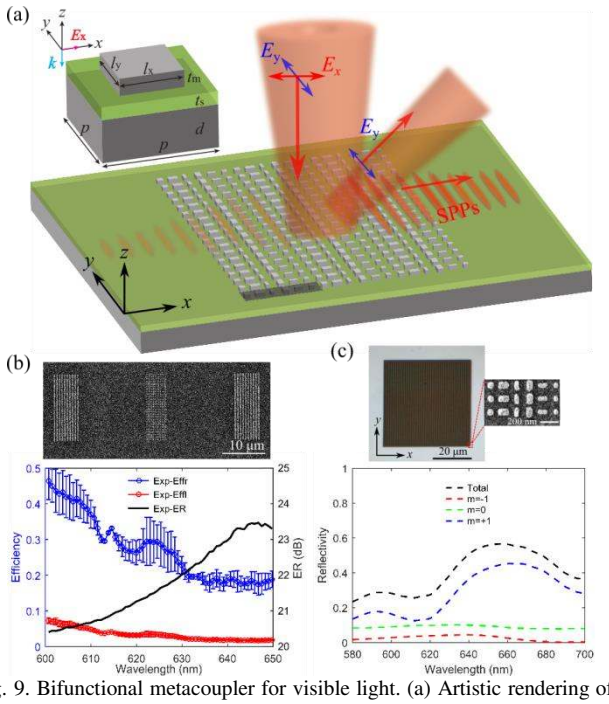

Fig. 9. Bifunctional metacoupler for visible light. (a) Artistic rendering of the working principle: different polarization components are selectively coupled into SPPs (x-polarization) or anomalously reflected (y-polarization). The gray region represents the supercell composed of six unit cells. (b) Optical measured coupling efficiencies and extinction ratio of the SPP coupling for x-polarization with an optimally positioned incident laser beam. The top panel shows the SEM image of the SPP coupling device. (c) Measured diffraction efficiencies of the metasurface as a broadband beam steerer for y-polarization. The top panel shows the SEM image of the sample. [91].

range of 580 – 700 nm with the corresponding steering angle varied from 30.6° to 37.9°, demonstrating the broadband steering for *y*-polarized light.

B. Spin-controlled Integrated Near-field and Far-field Optical Metacoupler

To further extend the functionalities of SPP metacouplers, a spin-controlled integrated near-field and far-field optical launcher has been proposed by Fang and co-works, which is capable of unidirectional launching SPPs in near-field and focusing scattered far-fields simultaneously [see Fig. 10(a)] [92]. The metacoupler consists of an array of subwavelength nanoslits with different orientations in gold film, which can generate locally PB-phase required to integrate the optical near-field and far-field functionalities in a single device under the CP incidence. Since the sign of the PB-phase is determined by the spin state of the incident CP light, the SPP propagating direction and the real/virtual focus of the far-field scattering can be manipulated by the spin of the incident light [30]. Fig. 10(b) shows the measured optical near-field intensities by using SNOM, manifesting the switchable unidirectional SPPs launching with the opposite CP incidence with different spins. Once the incident light is switched from LCP to RCP, the unidirectional propagation direction of generated SPPs will be altered from right-side to left-side. The estimated extinction ratios are found to be about 8 and 14 for the LCP and RCP incidences, respectively, which are in good agreement with the simulated values of 22 and 18.2, indicating the excellent performance of unidirectional SPP excitation. Apart from controlled SPPs excitation in the near-field, the proposed dual-functional metacoupler can work as a spin-controlled metalens, which possesses switchable real/virtual focus in the far-field. A real (virtual) focus at the transmitted (incident) side along the principal axis of light propagation with $z = 20$ μm ($z = -20$ μm) is clearly observed for LCP (RCP) incidence in Fig. 10(c), consistent with the previously demonstrated dual-polarity metalens based on PB-phase. Here it should be pointed out that the designed dual-functionalities do not interact with each other and each function maintains good optical performance.

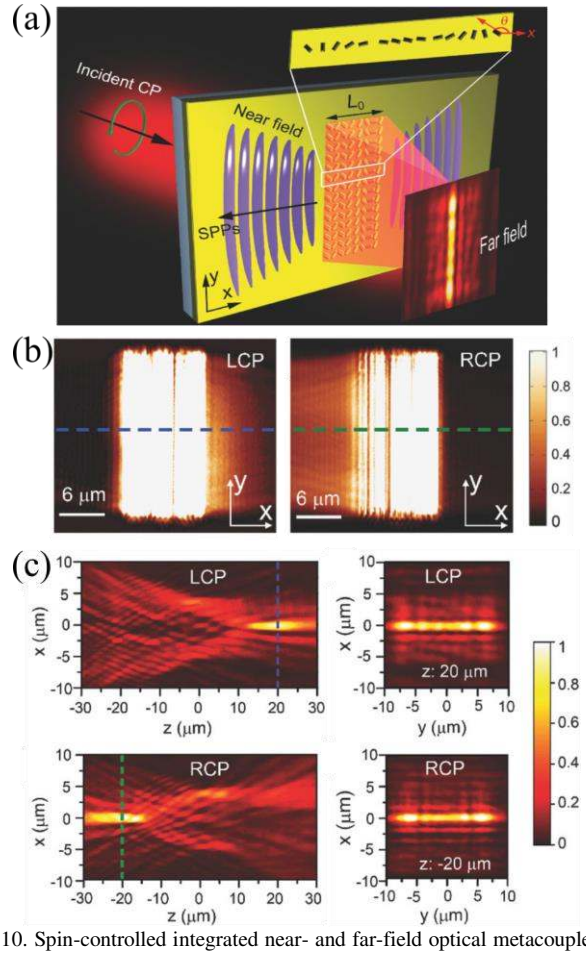

Fig. 10. Spin-controlled integrated near- and far-field optical metacoupler. (a) Schematic of the integrated near- and far-field metacoupler based on PB-phase metasurface composed of an array of nanoslits. (b) Measured optical near-field intensities with LCP and RCP incidences. (c) Measured optical far-field intensities at different planes with LCP and RCP incidences. [92].

V. Conclusion and Outlook

To summarize, we have briefly reviewed the recent achievements in the specific domain of gradient metasurface-based applications that is pertained to unidirectional SPP metacouplers. We have also outlined the general physics of phase discontinuities and generalized Snell's law, the basic concepts of metacouplers, the implementation of polarization-controlled tunable SPP metacouplers and multifunctional metacouplers that feature functions beyond the unidirectional SPP excitation.

Owing to the unprecedented capability of manipulating both the PWs and SWs and rapid developments in the area of metasurfaces, SPP metacouplers could further be developed progressing farther and beyond the status presented in this review article. Below we would like to mention some future directions in the field of metasurface-based SPP couplers.

(1) Metacouplers with 100% efficiency: Although numerous excellent examples of high-efficiency metacouplers have been demonstrated so far, the practical efficiency that could reach is still limited, especially at optical range, essentially because the excited SW propagates along the metacoupler surface and inevitably scatters out of the surface plane. Recently, several groups have proposed new strategies to steer an incident beam to an arbitrary direction with 100% efficiency by using properly-engineered bianisotropic meta-atoms [93], [94] or strong nonlocal metasurfaces [95]. We expect that this approach can further be extended aiming to achieve the PW-to-SW transformation with unitary efficiency. Another possibility would be to use artificial intelligence based algorithms, such as deep learning, to design and optimize the metacouplers in a reverse way [96], [97].

(2) Metacouplers enabling direct control over SPPs: In addition to efficiently launching SPPs from PWs, metasurfaces have also been widely used to control the wavefront of SPPs [98]–[103]. For example, spin-controlled SPP focusing has been achieved by PB-phase metasurface composed of apertures in metallic film, which suffer from low-efficiency [100], [101]. To increase the efficiency, Sun and co-works used a gradient-index metasurface slab on top of a plasmonic surface to reshape the wavefronts of the incident SPPs with the efficiency of SPP-steering reaching as high as ~70% [104]. Owing to the integration compatibility,

SPP metacouplers may find their use in high-performance, compact and integrated plasmonic circuits.

REFERENCES

[1] S. A. Maier, *Plasmonics: Fundamentals and Applications.* NewYork, USA: Springer, 2007.

[2] W. L. Barnes, A. Dereux, and T. W. Ebbesen, "Surface plasmon subwavelength optics," *Nature*, vol. 424, pp. 824, Aug. 2003.

[3] D. K. Gramotnev, and S. I. Bozhevolnyi, "Plasmonics beyond the diffraction limit," *Nat. Photon.*, vol. 4, pp. 83, Jan. 2010.

[4] J. A. Schuller *et al.*, "Plasmonics for extreme light concentration and manipulation," *Nat. Materials*, vol. 9, pp. 193, Feb. 2010.

[5] J. B. Pendry, L. Martín-Moreno, and F. J. Garcia-Vidal, "Mimicking surface plasmons with structured surfaces," *Science*, vol. 305, no. 5685, pp. 847, 2004.

[6] S. A. Maier, S. R. Andrews, L. Martín-Moreno, and F. J. Garcia-Vidal, "Terahertz surface plasmon-polariton propagation and focusing on periodically corrugated metal wires," *Phys. Rev. Lett.*, vol. 97, no. 17, pp. 176805, Oct. 2006.

[7] Q. Gan, Z. Fu, Y. J. Ding, and F. J. Bartoli, "Ultrawide-bandwidth slow-light system based on THz plasmonic graded metallic grating structures," *Phys. Rev. Lett.*, vol. 100, no. 25, pp. 256803, Jun. 2008.

[8] M. J. Lockyear, A. P. Hibbins, and J. R. Sambles, "Microwave surface-plasmon-like modes on thin metamaterials," *Phys. Rev. Lett.*, vol. 102, no. 7, pp. 073901, Feb. 2009.

[9] I. P. Radko *et al.*, "Efficient unidirectional ridge excitation of surface plasmons," *Opt. Express*, vol. 17, no. 9, pp. 7228-7232, Apr. 2009.

[10] N. Yu *et al.*, "Light propagation with phase discontinuities: generalized laws of reflection and refraction," *Science*, vol. 334, no. 6054, pp. 333, 2011.

[11] N. I. Zheludev, and Y. S. Kivshar, "From metamaterials to metadevices," *Nat. Mater.*, vol. 11, pp. 917, Oct. 2012.

[12] A. V. Kildishev, A. Boltasseva, and V. M. Shalaev, "Planar photonics with metasurfaces," *Science*, vol. 339, no. 6125, 2013.

[13] N. Yu *et al.*, "Flat optics: controlling wavefronts with optical antenna metasurfaces," *IEEE J. Sel. Top. Quantum Electron.*, vol. 19, no. 3, pp. 4700423-4700423, 2013.

[14] N. Yu, and F. Capasso, "Flat optics with designer metasurfaces," *Nat. Mater.*, vol. 13, pp. 139, Jan. 2014.

[15] H. Chen, A. J. Taylor, and N. Yu, "A review of metasurfaces: physics and applications," *Rep. Prog. Phys.*, vol. 79, no. 7, pp. 076401, 2016.

[16] G. Li, S. Zhang, and T. Zentgraf, "Nonlinear photonic metasurfaces," *Nat. Rev. Mater.*, vol. 2, pp. 17010, Mar. 2017.

[17] F. Ding, A. Pors, and S. I. Bozhevolnyi, "Gradient metasurfaces: a review of fundamentals and applications," *Rep. Prog. Phys.*, vol. 81, no. 2, pp. 026401, 2018.

[18] S. Chen, Z. Li, Y. Zhang, H. Chen, and J. Tian, "Phase manipulation of electromagnetic waves with metasurfaces and its applications in nanophotonics," *Adv. Opt. Mater.*, vol. 6, no. 13, pp. 1800104, Jul. 2018.

[19] M. C. Sajid *et al.*, "Material platforms for optical metasurfaces," *Nanophotonics*, vol. 7, no. 6, pp. 959, 2018.

[20] F. Ding, Y. Yang, A. D. Rucha, and S. I. Bozhevolnyi, "A review of gap-surface plasmon metasurfaces: fundamentals and applications," *Nanophotonics*, vol. 7, no. 6, pp. 1129, 2018.

[21] Q. He, S. Sun, S. Xiao, and L. Zhou, "High-efficiency metasurfaces: principles, realizations, and applications," *Adv. Opt. Mater.*, to be published. DOI: https://doi.org/10.1002/adom.201800415.

[22] S. Tang *et al.*, "Multifunctional metasurfaces based on the "merging" concept and anisotropic single-structure meta-atoms," *Appl. Sci.*, vol. 8, no. 4, pp. 555, 2018.

[23] X. Ni, N. K. Emani, A. V. Kildishev, A. Boltasseva, and V. M. Shalaev, "Broadband light bending with plasmonic nanoantennas," *Science*, vol. 335, no. 6067, pp. 427, 2012.

[24] F. Aieta *et al.*, "Out-of-plane reflection and refraction of light by anisotropic optical antenna metasurfaces with phase discontinuities," *Nano Lett.*, vol. 12, no. 3, pp. 1702-1706, Mar. 2012.

[25] S. Sun *et al.*, "High-efficiency broadband anomalous reflection by gradient meta-surfaces," *Nano Lett.*, vol. 12, no. 12, pp. 6223-6229, Dec. 2012.

[26] A. Pors, O. Albrektsen, I. P. Radko, and S. I. Bozhevolnyi, "Gap plasmon-based metasurfaces for total control of reflected light," *Sci. Rep.*, vol. 3, pp. 2155, Jul. 2013.

[27] A. Pors, F. Ding, Y. Chen, I. P. Radko, and S. I. Bozhevolnyi, "Random-phase metasurfaces at optical wavelengths," *Sci. Rep.*, vol. 6, pp. 28448, Jun. 2016.

[28] E. Hasman, V. Kleiner, G. Biener, and A. Niv, "Polarization dependent focusing lens by use of quantized Pancharatnam–Berry phase diffractive optics," *Appl. Phys. Lett.*, vol. 82, no. 3, pp. 328-330, Jan. 2003.

[29] F. Aieta *et al.*, "Aberration-free ultrathin flat lenses and axicons at telecom wavelengths based on plasmonic metasurfaces," *Nano Lett.*, vol. 12, no. 9, pp. 4932-4936, Sep. 2012.

[30] X. Chen *et al.*, "Dual-polarity plasmonic metalens for visible light," *Nat. Commun.*, vol. 3, pp. 1198, Nov. 2012.

[31] X. Ni, S. Ishii, A. V. Kildishev, V. M. Shalaev, "Ultra-thin, planar, Babinet-inverted plasmonic metalenses," *Light: Sci. Appl.*, vol. 2, pp. e72, Apr. 2013.

[32] A. Pors, M. G. Nielsen, R. L. Eriksen, and S. I. Bozhevolnyi., "Broadband focusing flat mirrors based on plasmonic gradient metasurfaces," *Nano Lett.*, vol. 13, no. 2, pp. 829-834, Feb. 2013.

[33] A. Arbabi, Y. Horie, A. J. Ball, M. Bagheri, and A. Faraon, "Subwavelength-thick lenses with high numerical apertures and large efficiency based on high-contrast transmitarrays," *Nat. Commun.*, vol. 6, pp. 7069, May. 2015.

[34] M. Khorasaninejad *et al.*, "Metalenses at visible wavelengths: diffraction-limited focusing and subwavelength resolution imaging," *Science*, vol. 352, no. 6290, pp. 1190, 2016.

[35] M. Khorasaninejad *et al.*, "Visible wavelength planar metalenses based on titanium dioxide," *IEEE J. Sel. Top. Quantum Electron.*, vol. 23, no. 3, pp. 43-58, 2017.

[36] M. S. Carstensen *et al.*, "Holographic resonant laser printing of metasurfaces using plasmonic template," *ACS Photonics*, vol. 5, no. 5, pp. 1665-1670, May. 2018.

[37] L. Huang *et al.*, "Three-dimensional optical holography using a plasmonic metasurface," *Nat. Commun.*, vol. 4, pp. 2808, Nov. 2013.

[38] X. Ni, A. V. Kildishev, and V. M. Shalaev, "Metasurface holograms for visible light," *Nat. Commun.*, vol. 4, pp. 2807, Nov. 2013.

[39] W. T. Chen *et al.*, "High-efficiency broadband meta-hologram with polarization-controlled dual images," *Nano Lett.*, vol. 14, no. 1, pp. 225-230, Jan. 2014.

[40] B. Desiatov, N. Mazurski, Y. Fainman, and U. Levy, "Polarization selective beam shaping using nanoscale dielectric metasurfaces," *Opt. Express*, vol. 23, no. 17, pp. 22611-22618, Aug. 2015.

[41] P. Genevet, and F. Capasso, "Holographic optical metasurfaces: a review of current progress," *Rep. Prog. Phys.*, vol. 78, no. 2, pp. 024401, 2015.

[42] G. Zheng *et al.*, "Metasurface holograms reaching 80% efficiency," *Nat. Nanotech.*, vol. 10, pp. 308, Feb. 2015.

[43] L. Huang, S. Zhang, and T. Zentgraf, "Metasurface holography: from fundamentals to applications," *Nanophotonics*, vol. 7, no. 6, pp. 1169, 2018.

[44] A. Pors, M. G. Nielsen, and S. I. Bozhevolnyi, "Broadband plasmonic half-wave plates in reflection," *Opt. Lett.*, vol. 38, no. 4, pp. 513-515, Feb. 2013.

[45] N. K. Grady *et al.*, "Terahertz metamaterials for linear polarization conversion and anomalous refraction," *Science*, vol. 340, no. 6138, pp. 1304, 2013.

[46] F. Ding, Z. Wang, S. He, V. M. Shalaev, and A. V. Kildishev, "Broadband high-efficiency half-wave plate: a supercell-based plasmonic metasurface approach," *ACS Nano*, vol. 9, no. 4, pp. 4111-4119, Apr. 2015.

[47] P. C. Wu *et al.*, "Versatile polarization generation with an aluminum plasmonic metasurface," *Nano Lett.*, vol. 17, no. 1, pp. 445-452, Jan. 2017.

[48] F. Ding, S. Zhong, and S. I. Bozhevolnyi, "Vanadium dioxide integrated metasurfaces with switchable functionalities at terahertz frequencies," *Adv. Opt. Mater.*, vol. 6, no. 9, pp. 1701204, May. 2018.

[49] A. Pors, M. G. Nielsen, and S. I. Bozhevolnyi, "Plasmonic metagratings for simultaneous determination of Stokes parameters," *Optica*, vol. 2, no. 8, pp. 716-723, Aug. 2015.

[50] J. P. Balthasar Mueller, K. Leosson, and F. Capasso, "Ultracompact metasurface in-line polarimeter," *Optica*, vol. 3, no. 1, pp. 42-47, Jan. 2016.

[51] E. Maguid *et al.*, "Photonic spin-controlled multifunctional shared-aperture antenna array," *Science*, vol. 352, no. 6290, pp. 1202, 2016.

[52] F. Ding, A. Pors, Y. Chen, V. A. Zenin, and S. I. Bozhevolnyi, "Beam-size-invariant spectropolarimeters using gap-plasmon metasurfaces," *ACS Photonics*, vol. 4, no. 4, pp. 943-949, Apr. 2017.

[53] Y. Chen, F. Ding, V. Coello, and S. I. Bozhevolnyi, "On-chip spectropolarimetry by fingerprinting with random surface arrays of nanoparticles," *ACS Photonics*, vol. 5, no. 5, pp. 1703-1710, May 2018.
[54] F. Ding, Y. Chen, and I. S. Bozhevolnyi, "Metasurface-based polarimeters," *Appl. Sci.*, vol. 8, no. 4, pp. 594, 2018.
[55] P. C. Wu *et al.*, "Visible metasurfaces for on-chip polarimetry," *ACS Photonics*, vol. 5, no. 7, pp. 2568-2573, Jul. 2018.
[56] F. López-Tejeira *et al.*, "Efficient unidirectional nanoslit couplers for surface plasmons," *Nat. Phys.*, vol. 3, pp. 324, Apr. 2007.
[57] J. Chen, Z. Li, S. Yue, and Q. Gong, "Efficient unidirectional generation of surface plasmon polaritons with asymmetric single-nanoslit," *Appl. Phys. Lett.*, vol. 97, no. 4, pp. 041113, Jul. 2010.
[58] C. Lu, X. Hu, H. Yang, and Q. Gong, "Ultrawide-band unidirectional surface plasmon polariton launchers," *Adv. Opt. Mater.*, vol. 1, no. 11, pp. 792-797, Nov. 2013.
[59] A. Baron *et al.*, "Compact antenna for efficient and unidirectional launching and decoupling of surface plasmons," *Nano Lett.*, vol. 11, no. 10, pp. 4207-4212, Oct. 2011.
[60] J. S. Q. Liu, R. A. Pala, F. Afshinmanesh, W. Cai, and M. L. Brongersma, "A submicron plasmonic dichroic splitter," *Nat. Commun.*, vol. 2, pp. 525, Nov. 2011.
[61] Y. Liu *et al.*, "Compact magnetic antennas for directional excitation of surface plasmons," *Nano Lett.*, vol. 12, no. 9, pp. 4853-4858, Sep. 2012.
[62] Z. Lei, and T. Yang, "Gap plasmon resonator arrays for unidirectional launching and shaping of surface plasmon polaritons," *Appl. Phys. Lett.*, vol. 108, no. 16, pp. 161105, Apr. 2016.
[63] S. Y. Lee *et al.*, "Role of magnetic induction currents in nanoslit excitation of surface plasmon polaritons," *Phys. Rev. Lett.*, vol. 108, no. 21, pp. 213907-1-213907-5, May 2012.
[64] F. J. Rodríguez-Fortuño *et al.*, "Near-field interference for the unidirectional excitation of electromagnetic guided modes," *Science*, vol. 340, no. 6130, pp. 328-330, Apr. 2013.
[65] J. P. B. Mueller and F. Capasso, "Asymmetric surface plasmon polariton emission by a dipole emitter near a metal surface," *Phys. Rev. B.*, vol. 88, pp. 121410-1—121410-6, Sep. 2013.
[66] S. Sun *et al.*, "Gradient-index meta-surfaces as a bridge linking propagating waves and surface waves", *Nat. Mater.*, vol. 11, pp. 426-431, Apr. 2012.
[67] C. Qu, S. Xiao, S. Sun, Q. He, and L. Zhou, "A theoretical study on the conversion efficiencies of gradient meta-surfaces," *Europhys. Lett.*, vol. 101, no. 5, pp. 54002, 2013.
[68] Z. Li *et al.*, "Controlling propagation and coupling of waveguide modes using phase-gradient metasurfaces," *Nat. Nanotech.*, vol. 12, pp. 675, Apr. 2017.
[69] C. Gong, J. Zhang, and S. He, "Hybrid unidirectional meta-coupler for vertical incidence to a high-refractive-index waveguide in telecom wavelength," *Opt. Lett.*, vol. 42, no. 24, pp. 5098-5101, Dec. 2017.
[70] W. Sun, Q. He, S. Sun, and L. Zhou, "High-efficiency surface plasmon meta-couplers: concept and microwave-regime realizations," *Light: Sci. Appl.*, vol. 5, pp. e16003, Jan. 2016.
[71] J. Lin *et al.*, "Polarization-controlled tunable directional coupling of surface plasmon polaritons," *Science*, vol. 340, pp. 331-334, 2013.
[72] F. J. Rodríguez-Fortuño *et al.*, "Near-field interference for the unidirectional excitation of electromagnetic guided modes," *Science*, vol. 340, pp. 328–330, 2013.
[73] A. E. Miroshnichenko, and Y. S. Kivshar, "Polarization traffic control for surface plasmons," *Science*, vol. 340, pp. 283–284, 2013.
[74] J. Yang *et al.*, "Broadband spin-controlled surface plasmon polariton launching and radiation via L-shaped optical slot nanoantennas," *Laser Photonics Rev.*, vol. 8, pp. 590–595, Jul. 2014.
[75] T. Tanemura *et al.*, "Multiple-wavelength focusing of surface plasmons with a nonperiodic nanoslit coupler", *Nano Lett.*, vol. 11, no. 7, pp. 2693-2698, Jul. 2011.
[76] J. P. B. Mueller, K. Leosson, and F. Capasso, "Polarization-selective coupling to long-range surface plasmon polariton waveguides," *Nano Lett.*, vol. 14, pp. 5524–5527, Oct. 2014.
[77] S. Pancharatnam, "Generalized theory of interference, and its applications," *Proc. Indian Acad. Sci. Sect.*, vol. 44, pp. 247–62, 1956.
[78] M. V. Berry, "Quantal phase factors accompanying adiabatic changes," *Proc. R Soc. A Math. Phy.s Eng. Sci.*, vol. 392, pp. 45–57, 1984.
[79] Z. E. Bomzon, V. Kleiner, and E. Hasman, "Pancharatnam–Berry phase in space-variant polarization-state manipulations with subwavelength gratings," *Opt. Lett.*, vol. 26, no. 18, pp. 1424-1426, Sep. 2001.
[80] G. Biener, A. Niv, V. Kleiner, and E. Hasman, "Formation of helical beams by use of Pancharatnam–Berry phase optical elements," *Opt. Lett.*, vol. 27, no. 21, pp. 1875-1877, Nov. 2002.
[81] Z. E. Bomzon, G. Biener, V. Kleiner, and E. Hasman, "Space-variant Pancharatnam–Berry phase optical elements with computer-generated subwavelength gratings," *Opt. Lett.*, vol. 27, no. 13, pp. 1141-1143, Jul. 2002.
[82] L. Huang *et al.*, "Helicity dependent directional surface plasmon polariton excitation using a metasurface with interfacial phase discontinuity," *Light: Sci. Appl.*, vol. 2, pp. e70, Mar. 2013.
[83] N. Shitrit, S. Maayani, D. Veksler, V. Kleiner, and E. Hasman, "Rashba-type plasmonic metasurface," *Opt. Lett.*, vol. 38, pp. 4358–4361, Nov. 2013.
[84] Q. Xuan *et al.*, "Efficient metacoupler for complex surface plasmon launching," *Adv. Opt. Mater.*, vol. 6, pp. 1701117, Mar. 2017.
[85] N. Shitrit, I. Yulevich, V. Kleiner, and E. Hasman, "Spin-controlled plasmonics via optical Rashba effect," *Appl. Phys. Lett.*, vol. 103, no. 21, pp. 211114, Nov. 2013.
[86] H. Mühlenbernd *et al.*, "Amplitude- and phase-controlled surface plasmon polariton excitation with metasurfaces," *ACS Photonics*, vol. 3, pp. 124–129, Jan 2016.
[87] J. Duan *et al.*, "High-efficiency chirality-modulated spoof surface plasmon meta-coupler," *Sci. Rep.*, vol. 7, pp. 1354, May 2017.
[88] A. Pors, M. G. Nielsen, T. Bernardin, J. C. Weeber, and S. I. Bozhevolnyi, "Efficient unidirectional polarization-controlled excitation of surface plasmon polaritons," *Light: Sci. Appl.*, vol. 3, pp. e197, Aug. 2014.
[89] A. Pors, and S. I. Bozhevolnyi, "Waveguide metacouplers for in-plane polarimetry," *Phys. Rev. Appl.*, vol. 5, no. 6, pp. 064015, Jun. 2016.
[90] T. Cai *et al.*, "High-performance bifunctional metasurfaces in transmission and reflection geometries," *Adv. Opt. Mater.*, vol. 5, no. 2, pp. 1600506, 2017.
[91] F. Ding, R. Deshpande, and S. I. Bozhevolnyi, "Bifunctional gap-plasmon metasurfaces for visible light: polarization-controlled unidirectional surface plasmon excitation and beam steering at normal incidence," *Light: Sci. Appl.*, vol. 7, pp. 17178, Apr. 2018.
[92] Q. Jiang *et al.*, "Spin-controlled integrated near- and far-field optical launcher," *Adv. Funct. Mater.*, vol. 28, no. 8, pp. 1705503, Feb. 2018.
[93] Y. Ra'di, D. L. Sounas, and A. Alù, "Metagratings: beyond the limits of graded metasurfaces for wave front control," *Phys. Rev. Lett.,* vol. 119, no. 6, pp. 067404, Aug. 2017.
[94] A. M. H. Wong, and G. V. Eleftheriades, "Perfect anomalous reflection with a bipartite Huygens' metasurface," *Phys. Rev. X,* vol. 8, no. 1, pp. 011036, Feb. 2018.
[95] A. Díaz-Rubio, V. S. Asadchy, A. Elsakka, and S. A. Tretyakov, "From the generalized reflection law to the realization of perfect anomalous reflectors," *Sci. Adv.,* vol. 3, no. 8, pp. e1602714, Aug. 2017.
[96] W. Ma, F. Cheng, and Y. Liu, "Deep-learning-enabled on-demand design of chiral metamaterials," *ACS Nano,* vol. 12, no. 6, pp. 6326-6334, Jun. 2018.
[97] J. Peurifoy *et al.*, "Nanophotonic particle simulation and inverse design using artificial neural networks," *Sci. Adv.,* vol. 4, no. 6, pp. eaar4206, Jun. 2018.
[98] L. Li, T. Li, S. Wang, S. Zhu, and X. Zhang, "Broad band focusing and demultiplexing of in-plane propagating surface plasmons," *Nano Lett.,* vol. 11, no. 10, pp. 4357-4361, Oct. 2011.
[99] D. Wintz, P. Genevet, A. Ambrosio, A. Woolf, and F. Capasso, "Holographic metalens for switchable focusing of surface plasmons," *Nano Lett.,* vol. 15, no. 5, pp. 3585-3589, May 2015.
[100] S. Xiao, F. Zhong, H. Liu, S. Zhu, and J. Li, "Flexible coherent control of plasmonic spin-Hall effect," *Nat. Commun.*, vol. 6, pp. 8360, Sep. 2015.
[101] X. Zhang *et al.*, "Anomalous surface wave launching by handedness phase control," *Adv. Mater.,* vol. 27, no. 44, pp. 7123-7129, 2015.
[102] S.-Y. Lee *et al.*, "Plasmonic meta-slit: shaping and controlling near-field focus," *Optica,* vol. 2, no. 1, pp. 6-13, Jan. 2015.
[103] S. S. Kou *et al.*, "On-chip photonic Fourier transform with surface plasmon polaritons," *Light: Sci. Appl.,* vol. 5, pp. e16034, Feb. 2016.
[104] S. Dong *et al.*, "Highly efficient wave-front reshaping of surface waves with dielectric metawalls," *Phys. Rev. Appl.,* vol. 9, no. 1, pp. 014032, Jan. 2018.

Fei Ding received his B.S. and Ph.D. degrees in optical engineering from Zhejiang University in 2010 and 2015, respectively. He is currently a postdoctoral fellow at Centre for Nano Optics at the University of Southern Denmark in Denmark. His current research interests are in the areas of nanophotonics, applied electromagnetics, metasurfaces, and plasmonics, and with particular focus on innovative and extreme aspects of wave interaction with engineered materials and nanostructures.

He is serving as a reviewer for several journals, he is currently the guest-editor of a special issue on metasurface for the journal of Applied Sciences. He was awarded the PIERS 2018 Toyama Yong Scientist Award in 2018.

Sergey I Bozhevolnyi received his M.Sc. Ph.D. degrees in quantum electronics from Moscow Institute of Physics and Technology (Russia) in 1978 and 1981, respectively. He was conferred the Dr. Sci. degree from Aarhus University, Aarhus, Denmark, in 1998 for the research on subwavelength light confinement. He initiated experimental research in near-field optics at the Institute of Physics, Aalborg University (Denmark) in 1991, where he has been Professor in 2003-2009 before moving to SDU. During 2001–2004, he was also the Chief Technical Officer (CTO) of Micro Managed Photons A/S set up to commercialize plasmonic waveguides.

He is currently a Professor and Head of Centre for Nano Optics at the University of Southern Denmark in Denmark. His current research interests include linear and nonlinear nano-optics and plasmonics, including plasmonic interconnects and metasurfaces.

He is a Fellow of Optical Society of America (2007) and a member of Danish Academy of Natural Sciences (2010).